

# Image Compression with Isotropic and Anisotropic Shepard Inpainting\*

Rahul Mohideen Kaja Mohideen<sup>1,\*</sup>, Tobias Alt<sup>1</sup>, Pascal Peter<sup>1</sup>, Joachim Weickert<sup>1</sup>

*Mathematical Image Analysis Group, Faculty of Mathematics and Computer Science  
Campus E1.7, Saarland University, 66041 Saarbrücken, Germany  
{rakaja, alt, peter, weickert}@mia.uni-saarland.de*

---

## Abstract

Inpainting-based codecs store sparse selected pixel data and decode by reconstructing the discarded image parts by inpainting. Successful codecs (coders and decoders) traditionally use inpainting operators that solve partial differential equations. This requires some numerical expertise if efficient implementations are necessary. Our goal is to investigate variants of Shepard inpainting as simple alternatives for inpainting-based compression. They can be implemented efficiently when we localise their weighting function. To turn them into viable codecs, we have to introduce novel extensions of classical Shepard interpolation that adapt successful ideas from previous codecs: Anisotropy allows direction-dependent inpainting, which improves reconstruction quality. Additionally, we incorporate data selection by subdivision as an efficient way to tailor the stored information to the image structure. On the encoding side, we introduce the novel concept of joint inpainting and prediction for isotropic Shepard codecs, where storage cost can be reduced based on intermediate inpainting results. In an ablation study, we show the usefulness of these individual contributions and demonstrate that they offer synergies which elevate the performance of Shepard inpainting to surprising levels. Our resulting approaches offer a more favourable trade-off between simplicity and quality than traditional inpainting-based codecs. Experiments show that they can outperform JPEG and JPEG2000 at high compression ratios.

*Keywords:* inpainting, image compression, Shepard interpolation, subdivision masks, anisotropic inpainting

---

\*This work has received funding from the European Research Council (ERC) under the European Union's Horizon 2020 research and innovation programme (grant agreement no. 741215, ERC Advanced Grant INCOVID)

\*Corresponding author

*Email addresses:* rakaja@mia.uni-saarland.de (Rahul Mohideen Kaja Mohideen), alt@mia.uni-saarland.de (Tobias Alt), peter@mia.uni-saarland.de (Pascal Peter), weickert@mia.uni-saarland.de (Joachim Weickert)

## 1. Introduction

While inpainting was introduced to restore missing or damaged regions of an image [1–3], inpainting-based compression [4, 5] is unconventional in two aspects: It drives inpainting to the extreme by considering very sparse data, and it combines it with data optimisation. In the encoding step, one stores only a small, carefully optimised fraction of the image pixels. During the decoding phase, the unknown data are approximated by inpainting. Since inpainting-like filling-in mechanisms are postulated to play an important role in the human visual system [6], inpainting-based compression appears natural and conceptually appealing. Moreover, aiming at sparsity in the spatial domain is particularly simple and distinguishes inpainting-based compression from widely-used transform-based approaches such as JPEG [7], JPEG2000 [8], and HEVC intra [9]. The latter ones aim at sparsity in the discrete cosine or wavelet domain. Advanced inpainting-based codecs can outperform JPEG2000 [5], and they can be far ahead of the state-of-the-art for data with a low to moderate amount of texture, such as depth maps [10].

Apart from a few notable exceptions such as exemplar-based inpainting [11], inpainting with concepts from Smoothed Particle Hydrodynamics [12], and linear spline inpainting [13–15], most inpainting-based codecs (coders and decoders) employ partial differential equations (PDEs) of diffusion type for inpainting. Homogeneous diffusion allows for very efficient algorithms if one uses sophisticated numerical ideas [16–21], while edge-enhancing anisotropic diffusion offers highest quality due to its anisotropy [4, 5].

Data optimisation has two aspects: One can optimise the positions of the stored pixels (*spatial optimisation*) as well as their corresponding grey or colour values (*tonal optimisation*). The positions of the stored pixels constitute the *inpainting mask*. While numerous methods have been proposed for spatial and tonal optimisation, there is a general trade-off between simplicity, efficiency, and quality.

The goal of our paper is to set a new benchmark in inpainting-based compression, that offers a better compromise than existing approaches w.r.t. simplicity of implementation, computational efficiency, and approximation quality. We aim at a family of simple and highly efficient codecs that does not require the numerical sophistication of PDE-based codecs, while keeping certain quality-critical features such as anisotropy and inpainting mask optimisation. It is based on variants of the classical Shepard interpolation idea [22].

Shepard interpolation relies on the idea of normalised weighted averaging. If one uses a localised weighting function, only a few surrounding mask pixels influence a given unknown pixel. The locality of the resulting Shepard inpainting allows simple and fast inpainting and tonal optimisation. This distinguishes it from PDE-based methods, where high efficiency in the inpainting step is possible but requires the adaptation of advanced numerical concepts such as multigrid techniques [16, 17], Fast Explicit Diffusion [23], Green’s functions [18,

20], finite element methods [19], and domain decomposition approaches [21]. Moreover, all exact methods for tonal optimisation of PDE-based approaches are relatively time-consuming and may be substantially slower than a fast PDE-based inpainting step. Shepard interpolation is non-iterative and requires little numerical expertise. While the original paper by Shepard [22] proposes inverse distance weighting functions without localisation, we use a variant from [24], which employs a truncated Gaussian weight function and only approximates the function values in the mask points. Since we perform tonal optimisation to maximise the approximation quality, this is unproblematic.

### 1.1. Our Contribution

Interestingly, despite its advantages, Shepard inpainting has not been explored for compression prior to our conference publication [25], where we have shown that it allows highly efficient image compression with reasonable quality. Its usefulness has also been confirmed for the compression of piecewise smooth images [10]. In the present work, we extend and improve our results from [25] by fusing the best of both worlds: the high efficiency from Shepard inpainting with two quality improvements from successful PDE-based codecs [4, 5], namely anisotropy and spatial mask adaptation. We also refine the work done in our conference publication by proposing a direct and more efficient tonal optimisation process for isotropic Shepard inpainting.

We propose a novel anisotropic version of Shepard inpainting which allows elongated Gaussian kernels to adapt the inpainting direction to the local image structure. Subdivision-based strategies enable us to find better inpainting data than just regular masks, but are not as expensive to store as fully optimised masks. For high compression ratios, our simple codec rivals the quality of transform-based approaches. In particular, it does not suffer from the pronounced block artefacts that plague the JPEG family [7, 8] at high compression rates.

When being localised, our Shepard inpainting codecs can offer substantial speed-ups over most implementations of PDE-based inpainting approaches. Our resulting methods are still simple and maintain a favourable trade-off between computational efficiency and reconstruction quality.

### 1.2. Related Work

In this section, we discuss prior work regarding the three pillars of each successful inpainting-based compression pipeline: inpainting operators, data selection strategies, and encoding.

**Inpainting Operators.** Since the inpainting operator recovers the missing image parts from the known data, it is crucial for the reconstruction quality. A significant number of operators use partial differential equations (PDEs). In particular, homogeneous diffusion [26] is a popular choice for compression [17, 27–31] since it is simple and fast compared to other PDE-based methods. It is an isotropic operator, i.e. it propagates information from stored pixels equally in all

directions. As a higher-order alternative to homogeneous diffusion, biharmonic inpainting [32] is another useful isotropic operator for sparse image inpainting [4, 5, 33]. Last but not least, anisotropic variants of nonlinear PDEs have been explored, most notably edge-enhancing diffusion (EED) [4, 34, 35] and higher-order variants [36, 37]. They adapt themselves to the local data structure. EED is the core component in some of the qualitatively best diffusion-based compression methods such as R-EED [5] and R-EED-LP [36].

While diffusion-based inpainting methods yield excellent results on piecewise smooth and mildly textured images, they struggle with high-frequency texture data. To address this issue, sparse exemplar-based inpainting methods have been proposed [38]. They reconstruct images by copying pixels or whole image patches from similar neighbourhoods. It is also possible to combine diffusion and exemplar-based inpainting methods in hybrid codecs [39].

Deep learning-based inpainting methods have also generated interest [40–42]. Successful concepts include generative adversarial networks (GANs) [43, 44] and deep priors approaches [45]. While deep learning approaches are undoubtedly powerful, they are computationally expensive to train and the models are not as transparent as PDE-based inpainting.

Shepard interpolation [22] is a simple and straightforward inpainting operator. It can be interpreted as a special case of a class of inpainting operators known as radial basis functions (RBFs) [46, 47] which have been successfully applied for scattered data interpolation [48–51]. Also, anisotropic variations of RBFs have been considered [12, 52, 53]. The work of Daropoulos et al. [12] is closest in spirit to our work, as they employ anisotropic RBF kernels with spatial and tonal optimisation.

Multiple publications have proposed improvements for isotropic Shepard interpolation. This includes restrictions of Shepard interpolation to a localised averaging of known data [54], which is also crucial for our own applications. This influence area of known data has also been adapted locally [55, 56].

In addition, strategies have been proposed to introduce directional information into Shepard interpolation. Tomczak [57] assigns higher averaging weights to points that are aligned along locally dominant directions, whereas Ringaby et al. [58] use anisotropic distance measures for image rectification. The approach of Lorenzi et al. [59] comes closest to our own anisotropic extension of Shepard interpolation. They define locally oriented ellipsoids in higher dimensions as averaging windows. However, compared to these previous methods, we benefit from the specific setting of our compression codec: instead of irregularly distributed known data, we define an anisotropic method on a regular grid. This allows more straightforward measures of anisotropy and a simple and elegant anisotropic extension of Shepard interpolation for the specialised purpose of compression. Shepard interpolation has been used successfully in sparse image inpainting [24, 60]. However, our conference publication [25] is the first that applies it to compression.

**Data Selection.** While the inpainting operator plays a very significant role in the final reconstruction quality, choosing the right data is equally important.

Spatial data optimisation can be broadly classified into two categories: unconstrained and constrained. Unconstrained mask selection approaches [19, 33, 44, 61–68] do not impose any structural restrictions on the mask pixel positions. This results in a mask which is completely optimised for the input image and the inpainting operator, which in turn results in the best possible reconstruction quality. However, from a coding viewpoint, this is not necessarily the best approach as storing these optimised positions can be very expensive. The compression of such unconstrained binary masks has been explored in detail in [69].

On the other hand, constrained mask approaches place mask points such that the positions have some structure or predictability to them. The simplest strategy of which is to place points on a regular grid. Other options include hexagonal grids with unconstrained mask points [27], and rectangular grids with edge information [10, 31]. When dealing with regular masks in this work, we also consider rectangular grids.

Subdivision-based approaches are another class of constrained mask approaches, where the mask is adapted to the image but the points are placed in a specific pattern. Usually, subdivision is implemented by splitting parts of the image with high error into smaller sub-images and placing more points where the reconstruction error is large. Earlier approaches such as [4, 13, 14] use a triangular subdivision, Later, Schmaltz et al. [5] proposed R-EED which employed rectangular subdivision, which was also used by R-EED-LP [36]. Subdivision allows image adaptivity while offering efficient storage in the form of trees. This motivates us to consider subdivision for our Shepard inpainting-based compression pipelines.

Optimising the grey or colour values of the known pixels is called tonal optimisation [62, 70]. The core principle of tonal optimisation is that errors are intentionally introduced in the known data such that the final reconstruction error is minimised. Related work on tonal optimisation will be discussed in Subsection 2.3.

**Encoding.** After the mask locations and the corresponding pixel values have been selected, we need to compress this information to reduce the final file size further. Inpainting-based compression pipelines have used PAQ [71] to great effect. PAQ is a family of entropy coders that employ context-mixing, wherein the symbol probabilities are calculated by combining probabilities from several similar symbol distributions that have been seen previously. In a way, we can interpret this procedure as trying to predict the next symbol which needs to be encoded. Prediction has been used in entropy coding to reduce file size [72]. It has also been integrated into the pipeline of popular image compression methods such as PNG [73] and H.265-intra [9].

However, for inpainting-based compression methods, prediction has only

been performed as a part of the entropy coding, and it has never been integrated into the pipeline. Therefore, in this work, we exploit the nature of the inpainting operator to predict pixels during compression and decompression. This results in our joint inpainting and prediction approach.

### 1.3. Organisation of the Paper

In Section 2, we review the basic components of inpainting-based compression. In Section 3, we introduce the anisotropic version of Shepard inpainting. After that, we present the full compression pipelines for our Shepard inpainting codecs in Section 4. Finally, we evaluate the performance of these new approaches in Section 5 and conclude our paper with a summary and an outlook on future work in Section 6.

## 2. Review: Inpainting-based Compression

Every inpainting-based compression approach requires a suitable inpainting method and a corresponding selection strategy for optimised known data. In this section, we review some of those approaches in more detail, and if they are either directly relevant to our own contributions. Moreover, we also discuss tonal optimisation as an additional way to optimise known data for better inpainting results.

### 2.1. Inpainting Methods

#### 2.1.1. Inpainting with Diffusion Processes

Diffusion has a long tradition in image processing [26, 74, 75] and it has also been used for image inpainting; see e.g. [29, 35]. Let  $f : \Omega \rightarrow \mathbb{R}$  denote a grey value image on a rectangular image domain  $\Omega \subset \mathbb{R}^2$  that is only known on a subset  $K \subset \Omega$ , also called the *inpainting mask*. To reconstruct the unknown image data in  $\Omega \setminus K$ , diffusion-based inpainting computes the steady state ( $t \rightarrow \infty$ ) of the following initial value problem:

$$\partial_t u = \operatorname{div}(\mathbf{D}\nabla u) \quad \text{on } \Omega \setminus K \times (0, \infty), \quad (1)$$

$$u(x, y, t) = f(x, y, 0) \quad \text{on } K \times [0, \infty), \quad (2)$$

$$\mathbf{n}^\top \mathbf{D}\nabla u = 0 \quad \text{on } \partial\Omega \times (0, \infty). \quad (3)$$

Here,  $u(x, y, t)$  denotes the image pixel value at position  $(x, y)$  and time  $t$ , and  $\mathbf{n}$  is the outer normal vector at the image boundary  $\partial\Omega$ . The spatial gradient operator is denoted by  $\nabla = (\partial_x, \partial_y)^\top$ , and  $\operatorname{div} = \nabla^\top$  is the divergence. The diffusion tensor  $\mathbf{D} \in \mathbb{R}^{2 \times 2}$  is a positive semi-definite matrix. Its eigenvectors determine the propagation directions of the diffusion process, and their eigenvalues determine the amount of diffusion along those directions. The Dirichlet boundary conditions in Eq. (2) specify that known pixel values stay unmodified. Reflecting boundary conditions are defined in Eq. (3) to avoid diffusion across the image boundaries.

The simplest choice for the diffusion tensor is  $\mathbf{D} = \mathbf{I}$ , where  $\mathbf{I}$  is the identity matrix. In that case, we can write Eq. (1) as

$$\partial_t u = \operatorname{div}(\nabla u) = \Delta u = \partial_{xx} u + \partial_{yy} u. \quad (4)$$

This equation describes *homogeneous diffusion* which propagates information isotropically in all directions [26].

There are more sophisticated choices for  $\mathbf{D}$  which also allow e.g. direction-dependent (anisotropic) inpainting adaptation. For example, *edge-enhancing anisotropic diffusion* (EED) [34, 35] considers the diffusion tensor  $\mathbf{D}(\nabla u_\sigma)$ , where  $u_\sigma$  represents the convolution of the evolving image  $u$  with a Gaussian kernel of standard deviation  $\sigma$ . This Gaussian convolution makes the edge detector  $|\nabla u_\sigma|^2$  more robust under noise, where  $|\cdot|$  denotes the Euclidean norm. The first normalised eigenvector of  $\mathbf{D}(\nabla u_\sigma)$  is chosen as  $\mathbf{v}_1 = \nabla u_\sigma / |\nabla u_\sigma|$ . It is perpendicular to the edge, while the second normalised eigenvector  $\mathbf{v}_2$  is parallel to it. The eigenvalues  $\mu_1, \mu_2$  denote the contrast in the direction of these eigenvectors. By setting  $\mu_2 = 1$ , one allows full diffusion along edges. To reduce diffusion across edges, one uses for  $\mu_1$  a decreasing diffusivity such as the one by Charbonnier et al. [76]:

$$\mu_1 = g(|\nabla u_\sigma|^2) = \frac{1}{\sqrt{1 + \frac{|\nabla u_\sigma|^2}{\lambda^2}}}. \quad (5)$$

with some contrast parameter  $\lambda > 0$ . With these choices,  $\mathbf{D}(\nabla u_\sigma)$  can be written as

$$\mathbf{D}(\nabla u_\sigma) = g(|\nabla u_\sigma|^2) \mathbf{v}_1 \mathbf{v}_1^\top + \mathbf{v}_2 \mathbf{v}_2^\top. \quad (6)$$

For inpainting with homogeneous diffusion or EED, one observes global convergence where the steady state does not depend on the initialisation. However, since a good initialisation can accelerate the convergence, a pragmatic approach is to initialise the non-mask pixels with the average grey value of the mask pixels.

For EED inpainting, one discretises the parabolic PDE (1) with finite differences and computes the reconstruction by means of numerical solvers [77]. An explicit time discretisation is simple but has to obey severe time step size restrictions for stability reasons. There are ways to accelerate explicit schemes by using cyclically varying time step sizes [78], or extrapolation ideas [79, 80]. A semi-implicit time discretisation does not suffer from any time step size limits [75], but requires solving a large linear system with a matrix that is symmetric, positive definite, and sparse. To this end, one can use iterative solvers such as conjugate gradients.

For homogeneous diffusion inpainting, efficient numerical solvers often exploit direct discretisations of the Laplace equation  $\Delta u = 0$  that arises in the steady state. This has been done with multigrid methods [16, 17], discrete

Green’s function approaches [18, 20], finite element discretisations with conjugate gradient solvers [19], and domain decomposition algorithms [21].

These discussions show that diffusion-based inpainting requires quite some numerical expertise, if one aims at highly efficient algorithms. This motivates us to study alternatives that also offer efficient algorithms, but do not rely on such an expertise and lead to fairly simple implementations.

### 2.1.2. Inpainting with Radial Basis Functions

For inpainting with radial basis functions [47, 49], we consider the same interpolation problem as in the previous section, where  $f : \Omega \rightarrow \mathbb{R}$  where known data is only given on the set  $K \subset \Omega$ . According to [46], this can be seen as a sparse interpolation problem that can be solved with a weighted averaging of the known data

$$u(\mathbf{x}_i) = \sum_{\mathbf{x}_j \in K} w(\mathbf{x}_j - \mathbf{x}_i) c_j. \quad (7)$$

Here,  $w$  denotes a radial basis function, for instance a multiquadric [49]. The unknown coefficients  $c_j$  of this interpolation approach are determined by the interpolation condition

$$u(\mathbf{x}_j) = f(\mathbf{x}_j) \quad \forall \mathbf{x}_j \in K. \quad (8)$$

Together with Eq. (7), these constraints establish a linear system of equations that needs to be solved to obtain the coefficients  $c_j$ . As soon as these are known, the inpainting result is obtained directly by weighted averaging.

### 2.1.3. Isotropic Shepard Inpainting

Shepard interpolation [22, 60] can be interpreted as a simplified special case of normalised RBF interpolation. In particular, no interpolation weights need to be computed, and an inpainted value  $u(\mathbf{x}_i)$  can be directly obtained as

$$u(\mathbf{x}_i) = \begin{cases} \frac{\sum_{\mathbf{x}_j \in K} w(\mathbf{x}_j - \mathbf{x}_i) f_j}{\sum_{\mathbf{x}_j \in K} w(\mathbf{x}_j - \mathbf{x}_i)}, & \text{if } \forall j : |\mathbf{x}_i - \mathbf{x}_j| > 0, \\ f_i, & \text{if } \exists j : |\mathbf{x}_i - \mathbf{x}_j| = 0. \end{cases} \quad (9)$$

The weighting function  $w$  penalises the distance of the known data at  $\mathbf{x}_j$  from the interpolated position  $\mathbf{x}_i$  according to

$$w(\mathbf{x}_j - \mathbf{x}_i) = \frac{1}{|\mathbf{x}_j - \mathbf{x}_i|^p}. \quad (10)$$

The parameter  $p > 1$  controls the influence of neighbouring points, where higher values of  $p$  result in less contributions from distant points. Comparing Eq. (7) and Eq. (9), the coefficients in Shepard interpolation are chosen as

$$c_j := \frac{f_j}{\sum_{\mathbf{x}_j \in K} w(\mathbf{x}_j - \mathbf{x}_i)}. \quad (11)$$

For our compression application, a variant of the original definition of Shepard interpolation is helpful. This Shepard inpainting eliminates the case distinction in Eq. (9) and performs the weighted averaging from the first case everywhere [24]. This relaxation implies that for known data, the interpolation condition is not necessarily met and thus our inpainting performs approximation instead of interpolation. In Sec. 2.3 we discuss why this choice is well-suited for our compression application. Moreover, in the following, we use Gaussian weights

$$G_\sigma(\mathbf{x}) := \exp(-|\mathbf{x}|^2/(2\sigma^2)) . \quad (12)$$

Note that such a Gaussian weighting function has infinite support, and thus every known data point in the image would be used for each averaging. For our fast and simple codec, it is crucial to truncate these Gaussians. By limiting the weighting window to  $(\lceil 4\sigma \rceil + 1) \times (\lceil 4\sigma \rceil + 1)$ , the computational effort is reduced to  $(O)(\sigma^2|K|)$ . In addition, this truncation allows us to provide closed-form solutions for important optimisation steps in our encoder in Section 4.1.

However, this truncation can lead to situations where the interpolation window does not contain any known data. To reduce this danger, we follow Achanta et al. [24], who adapt the standard deviation to the fraction of known data according to

$$\sigma = \sqrt{(m \cdot n)/(\pi|K|)} . \quad (13)$$

Here  $m$  and  $n$  denote the dimensions of the discrete image, and  $|K|$  is the number of mask pixels. This leads us to the final equation for Shepard inpainting of  $u_i = u(\mathbf{x}_i)$ :

$$u_i = \frac{\sum_{\mathbf{x}_j \in K} G_\sigma(\mathbf{x}_j - \mathbf{x}_i) f_j}{\sum_{\mathbf{x}_j \in K} G_\sigma(\mathbf{x}_j - \mathbf{x}_i)} . \quad (14)$$

Note that the weighting function only depends on the distance between the two pixels and not its orientation. Thus, we refer to this strategy as *isotropic* Shepard inpainting. In Section 3, we extend this to an *anisotropic* concept with oriented Gaussians which distribute information along dominant image structures.

## 2.2. Choosing Mask Points

Spatial data selection has a large influence on the final reconstruction of an inpainting-based compression method. We can employ a variety of methods to select the known pixels. Basic strategies rely on non-adaptive masks. For instance, they use a regular mask which places points on a uniform grid, or a (pseudo-)random mask. Both options require little to no storage cost, as we need to store only the grid size for regular masks or the seed value for the pseudo-random generator in the case of random masks.

There are also fully adaptive masks which do not have any constraints on mask point positions but are very expensive to store [69]. Finding such adaptive masks constitutes a challenging optimisation problem which is addressed by

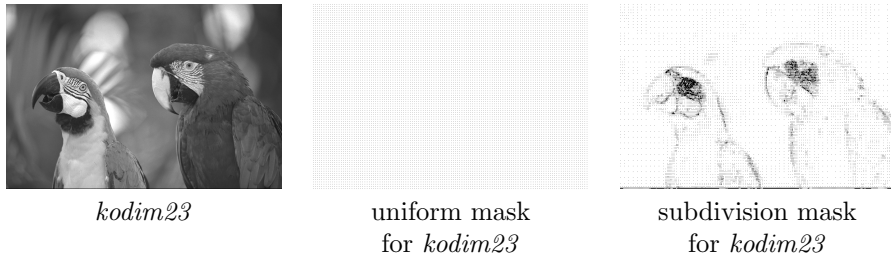


Figure 1: Uniform masks do not adapt to the image structure but generate no overhead. On the contrary, subdivision can be used to create masks that are adaptive to the image structure and can be stored easily with trees. The black pixels in the mask image are the known data points.

many diverse approaches [19, 61–65, 81–83]. Recently, also deep learning has been explored to optimise locations of known data [66, 68].

Subdivision masks [5, 13, 36] offer a compromise between the two extremes mentioned above. They offer a good trade-off between spatial adaptivity and ease of compression. Subdividing the image and storing points at fixed positions in these subimages reduces the storage cost significantly. An example subdivision mask can be seen in Fig. 1.

Since we aim for simple and fast codecs, we use only non-adaptive and subdivision masks in the following.

### 2.3. Tonal Optimisation

In addition to choosing the location of mask pixels, it is also possible to optimise their value. This is referred to as tonal optimisation [62, 70, 84]. It modifies the known pixel values such that the global mean squared error (MSE) is minimised. Even though this introduces errors in the sparse stored data, this is outweighed by significant reconstruction improvements in the large unknown areas.

Since the known data is no longer reliable, it makes sense to relax the interpolation condition. Therefore, we choose approximation over interpolation for our inpainting. Previous approaches have addressed this issue with post-processing instead [5]. In addition to tonal optimisation, there are more sources for errors in known data: noise and quantisation. Coarse quantisation intentionally reduces the number of admissible pixel values in the grey-level domain, hence reducing storage costs. Quantisation can be applied as post-processing after tonal optimisation but might revert some of its improvements. Thus, it is often preferred to account for quantisation already during the tonal optimisation.

For linear inpainting operators such as homogeneous diffusion, we can write the tonal optimisation problem as an energy minimisation problem, and there are various strategies to solve it. A detailed review of these strategies can be found in [68].

A simple but effective tonal optimisation method that can be applied to all deterministic inpainting operators relies on the principle of trial and error. It visits known pixels in a random order and adjusts their quantised values to a higher or lower level. Changes that yield a lower inpainting error [5] are kept. This method is widely applicable and takes quantisation into account directly, but also often entails a high cost since every quality check requires an image inpainting. In Section 4.1, we show that in combination with Shepard inpainting, this method can be highly effective.

### 3. Anisotropic Shepard Inpainting

Shepard inpainting uses isotropic Gaussian functions which are rotationally invariant. Thus, information from known pixels is propagated equally in all directions. However, additional directional information is implicitly encoded in the known pixels, and the use of such data has been successful in anisotropic diffusion inpainting [4, 35]. This motivates us to combine the speed and simplicity of Shepard inpainting with ideas from edge enhancing diffusion (EED) [34].

To this end, we introduce *anisotropic Shepard inpainting*, which allows the weighting function to adapt to the local directional structure of the available data. We compute gradient information from the available data and, in the same fashion as EED, use this information to guide the influence function accordingly. Thus, we achieve an anisotropic inpainting effect. In particular, when the known data are arranged in a regular fashion, we can compute the gradient information without any overhead.

We propose to modify the weighting function  $w$  based on structural information which is encoded in the vector containing the mask pixels  $\mathbf{f} \in \mathbb{R}^{mn}$  for an image of resolution  $m \times n$ . To this end, we adapt the weighting function at each mask position  $\mathbf{x}_j \in K$  to obtain a set of functions  $w_j$ . Our anisotropic Shepard inpainting computes the reconstruction  $u_i$  as

$$u_i = \frac{\sum_{\mathbf{x}_j \in K} w_j(\mathbf{x}_j - \mathbf{x}_i) f_j}{\sum_{\mathbf{x}_j \in K} w_j(\mathbf{x}_j - \mathbf{x}_i)}. \quad (15)$$

The spatially varying weighting functions  $w_j$  depend on the local structure of the masked image  $\mathbf{f}$ .

For simplicity, we now switch to the continuous case and consider a greyscale image  $f : \Omega \rightarrow \mathbb{R}$  which is fully available on a continuous domain  $\Omega \subset \mathbb{R}^2$ . The gradient  $\nabla f$  encodes the structural information of  $f$  which allows to define structure-adaptive weighting functions.

As a weighting function we choose an oriented Gaussian with standard deviations  $\sigma_1, \sigma_2$ , and a rotation angle  $\theta$ . The two standard deviations  $\sigma_1, \sigma_2$  determine the major and minor directions of the Gaussian. For  $\sigma_1 = \sigma_2$ , we want to obtain a rotationally invariant Gaussian corresponding to the isotropic case.

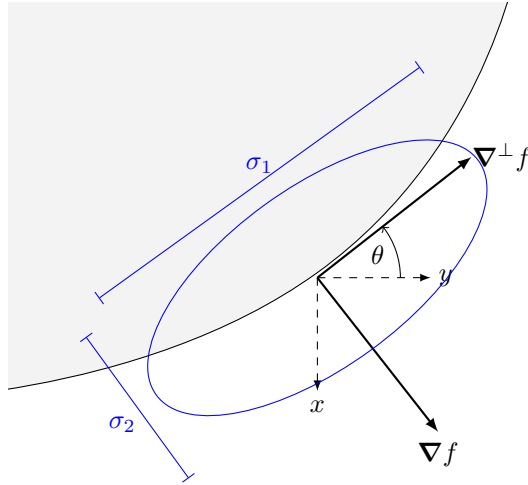


Figure 2: Local adaptation of the weighting function to the image structure in a continuous setting. The gradient  $\nabla f$  spans a coordinate system rotated by  $\theta$  w.r.t. the  $(x, y)$ -system. The gradient magnitude shrinks the level lines of the Gaussian kernel (blue) across dominant structures. This gives elliptic level lines with major and minor axes proportional to  $\sigma_1$  and  $\sigma_2$ , respectively.

A model which fulfils the above properties based on the structural information described by the image gradient  $\nabla f = (f_x, f_y)^\top$  in the  $(x, y)$ -coordinate system is given by

$$\sigma_1^2 = \sigma^2, \quad (16)$$

$$\sigma_2^2 = g(|\nabla f|^2) \sigma^2, \quad (17)$$

$$\theta = \arctan\left(-\frac{f_x}{f_y}\right), \quad (18)$$

where  $\sigma$  is an input parameter determining the base standard deviation of the Gaussian as in the isotropic case. Note that  $\sigma_1$  and  $\sigma_2$  are functions of  $\sigma$  and  $\nabla f$ , but have been abbreviated for readability. In Fig. 2, we visualise the relation between these parameters in a continuous setting.

In our experiments, we found the rational Perona–Malik diffusivity [74]

$$g(s^2) = \frac{1}{1 + \frac{s^2}{\lambda^2}} \quad (19)$$

to be a suitable choice. It attenuates the variance  $\sigma^2$  at image locations with dominant structures where the edge detector  $|\nabla f|$  exceeds some contrast parameter  $\lambda$ . Choosing the constant diffusivity [26]  $g(s^2) = 1$  returns the isotropic Shepard inpainting model.

The angle  $\theta$  determines the rotation of the anisotropic Gaussian function. As  $\nabla f$  points into the direction of the steepest ascent of  $f$ , the anisotropic Gaussian should be oriented along the orthogonal direction  $\nabla^\perp f$ . In 2D, a vector which is orthogonal to the gradient can be easily constructed, e.g. as  $\nabla^\perp f = (f_x, -f_y)^\top$ . The angle of this vector in the respective coordinate system is given by  $\theta$  in Eq. (18).

In the  $(\nabla^\perp f, \nabla f)$ -coordinate system, the resulting Gaussian weighting function should scale the kernel along the principal directions by the standard deviations  $\sigma_1, \sigma_2$  given above. Thus, we obtain

$$\mathbf{z}^\top \boldsymbol{\Sigma} \mathbf{z} = \begin{pmatrix} z_1 & z_2 \end{pmatrix} \begin{pmatrix} \frac{1}{2\sigma_1^2} & 0 \\ 0 & \frac{1}{2\sigma_2^2} \end{pmatrix} \begin{pmatrix} z_1 \\ z_2 \end{pmatrix} \quad (20)$$

as an argument for the Gaussian function, where  $\mathbf{z}$  is the spatial difference between two positions in the  $(\nabla^\perp f, \nabla f)$ -coordinate system.

Let us now bring this argument to the  $(x, y)$ -coordinate system. To this end, we multiply a rotation by  $\theta$  from the right, and its inverse from the left, yielding

$$\mathbf{R}_\theta^{-1} \mathbf{z}^\top \boldsymbol{\Sigma} \mathbf{z} \mathbf{R}_\theta = \mathbf{d}^\top \mathbf{R}_\theta^{-1} \boldsymbol{\Sigma} \mathbf{R}_\theta \mathbf{d}. \quad (21)$$

Here,  $\mathbf{d}$  is the spatial distance between two positions in the  $(x, y)$ -coordinate system. Note that we used the relation  $\mathbf{z} = \mathbf{R}_\theta \mathbf{d}$  to move the rotation matrices inside the expression.

Expressing the inner matrix with parameters  $\alpha, \beta, \gamma$ , we obtain

$$\begin{pmatrix} \alpha & \beta \\ \beta & \gamma \end{pmatrix} = \mathbf{R}_\theta^{-1} \boldsymbol{\Sigma} \mathbf{R}_\theta \quad (22)$$

which, by additionally using the identity  $\cos(\theta) \sin(\theta) = \frac{1}{2} \sin(2\theta)$  yields

$$\alpha(\theta, \sigma_1, \sigma_2) = \frac{\cos^2(\theta)}{2\sigma_1^2} + \frac{\sin^2(\theta)}{2\sigma_2^2}, \quad (23)$$

$$\beta(\theta, \sigma_1, \sigma_2) = -\frac{\sin(2\theta)}{4\sigma_1^2} + \frac{\sin(2\theta)}{4\sigma_2^2}, \quad (24)$$

$$\gamma(\theta, \sigma_1, \sigma_2) = \frac{\sin^2(\theta)}{2\sigma_1^2} + \frac{\cos^2(\theta)}{2\sigma_2^2}. \quad (25)$$

The resulting Gaussian weighting function takes the distance between two spatial positions  $\mathbf{d} = (d_1, d_2)^\top = \mathbf{x} - \mathbf{y}$  and computes

$$G_{\theta, \sigma_1, \sigma_2}(\mathbf{d}) = \exp(-\alpha d_x^2 + 2\beta d_x d_y - \gamma d_y^2), \quad (26)$$

where  $\alpha, \beta$  and  $\gamma$  are functions of  $\theta, \sigma_1$  and  $\sigma_2$ .

## 4. Compression Pipeline

### 4.1. Regular Grid Codec with Isotropic Shepard inpainting

As a first method that aims for maximal simplicity, we propose the *regular grid codec with joint inpainting and prediction* (RJIP), which we presented in our conference publication [25]. While it is not image adaptive, it exploits novel prediction principles with inpainting instead. We store the known data on a regular mask, which means the only storage cost for positional data is the grid size parameter  $r$ . This generates minimal overhead. For the grey value data corresponding to the mask positions, we use an equally straightforward uniform scalar quantisation: We map the 8 bit colour values to a reduced range range  $\{0, \dots, q - 1\}$  by partitioning the tonal domain into  $q$  subintervals of equal length.

Shepard inpainting from Eq. (14) is implemented by visiting each mask point  $\mathbf{x}_j \in K$  and adding its impact on the reconstruction. The contribution to the numerator is stored in the value accumulation map  $\mathbf{v}$  and the contribution to the denominator is stored in the weight accumulation map  $\mathbf{w}$ . For  $w_i := w(\mathbf{x}_i)$  and  $v_i := v(\mathbf{x}_i)$ , both maps are then updated as follows:

$$w_i \leftarrow w_i + G_\sigma(\mathbf{x}_i - \mathbf{x}_j), \quad (27)$$

and

$$v_i \leftarrow v_i + G_\sigma(\mathbf{x}_i - \mathbf{x}_j) f_j \quad (28)$$

for all points  $\mathbf{x}_i$  in the truncated Gaussian neighbourhood  $\mathcal{N}_j$  of  $\mathbf{x}_j \in K$ . The new inpainting at point  $\mathbf{x}_i$  can then be computed as

$$u_i = v_i / w_i. \quad (29)$$

To further decrease the final compressed file size, RJIP employs *joint inpainting and prediction*. In general, often better coding efficiency can be achieved by predicting the future values to be stored from already encoded data. Instead of the values themselves, we can encode the prediction error, the so-called *residuals*, instead. Good predictions yield residuals that cluster around zero, thus reducing entropy, which directly translates to reduced storage cost.

We integrate this idea seamlessly into Shepard inpainting. During image compression, the mask points are traversed one-by-one. If the weight accumulation map  $w$  is non-zero at the location the next mask point to be encoded, an initial prediction can be computed through

$$p_i = v_i / w_i. \quad (30)$$

Then we encode the residual between the prediction and the actual mask value as

$$e_i = (p_i - f_i) \bmod q. \quad (31)$$

Using a sufficiently large Gaussian as in Eq. (13) ensures that each new encoded data point can predict at least one data point that has not yet been encoded. After the mask point is encoded, we update the value and accumulation maps and repeat until all points are encoded. We finally compress the residuals with a suitable entropy coder. RJIP relies on *finite state entropy* (FSE) [85], a fast coder similar to arithmetic coding [86].

For a given compression ratio, RJIP chooses the parameters  $r$  and  $q$  through a golden-section search such that the best reconstruction quality for the desired file size is obtained. While the iterative random walk method that we discussed in Section 2.3 is already well-suited for Shepard inpainting due to its locality, it even allows a closed-form solution for the tonal optimisation of individual pixels.

In the following,  $u_i^{\text{old}}$  and  $u_i^{\text{new}}$  are the old and new pixel value at  $\mathbf{x}_i \in K$ . We want to find  $u_i^{\text{new}}$ , such that it minimises the *mean squared error* (MSE). Then the new error after updating  $u_i^{\text{old}}$  to  $u_i^{\text{new}}$  is given by [87]

$$e(u_i^{\text{new}}) = \sum_{\mathbf{x}_j \in \mathcal{N}_i} \left( f_j - \frac{v_j + G_\sigma(\mathbf{x}_j - \mathbf{x}_i)(u_i^{\text{new}} - u_i^{\text{old}})}{w_j} \right)^2, \quad (32)$$

where  $\mathcal{N}_i$  is the neighbourhood of points around  $\mathbf{x}_i$ ,  $v_j$  and  $w_j$  are the value accumulation map and the weight accumulation map from Eq. (14),  $G_\sigma$  is the Gaussian defined in Eq. (12), and  $f_j$  is the ground truth value at  $\mathbf{x}_j$ . Intuitively, the error can be computed by subtracting the weighted old mask value in the neighbourhood and adding the weighted new mask value.

An optimal tonal value should minimise this error. As the error function described in Eq. (32) is convex, an optimal tonal value is obtained by the condition  $\frac{d}{du_i^{\text{new}}} e(u_i^{\text{new}}) = 0$ . This yields the closed-form solution

$$u_i^{\text{new}} = \frac{\sum_{\mathbf{x}_j \in \mathcal{N}_i} \frac{G_\sigma(\mathbf{x}_j - \mathbf{x}_i)}{w_j} \left( f_j - \frac{v_j - G_\sigma(\mathbf{x}_j - \mathbf{x}_i)u_i^{\text{old}}}{w_j} \right)}{\sum_{\mathbf{x}_j \in \mathcal{N}_i} \frac{G_\sigma(\mathbf{x}_j - \mathbf{x}_i)^2}{w_j^2}}. \quad (33)$$

It enables us to directly compute the optimal tonal value at a mask point. Then we project the obtained optimal values to the set of quantised values. Iterating these computations over all mask points multiple times converges to optimised mask values. As we do not have to compute the inpainting for the full image every time we change a pixel value, the tonal optimisation for isotropic Shepard inpainting is highly efficient.

#### 4.2. Subdivision Codec with Anisotropic Shepard inpainting

Subdivision masks offer a good balance between image adaptivity, coding costs, and complexity, which make them an attractive component of our codecs. We adopt this concept from Schmaltz et al. [5] by starting with the whole image as a single block and placing a mask point in each corner of the image. If the reconstruction error in a block is higher than a threshold parameter, we split

the block in two along its largest dimension and add mask points at each corner of the smaller blocks. This process is then repeated until all blocks have a reconstruction error lower than the given threshold. We can then store the splitting decisions in the form of a binary tree which has a low coding cost.

To overcome the issue of approximating derivatives on a non-uniform grids, we first perform an isotropic Shepard inpainting on the mask and then compute derivatives with a sampling distance of one on the inpainted image. Then we use these derivatives to compute the final anisotropic inpainting.

Uniform mask codecs use a global Gaussian standard deviation  $\sigma$  in Eq. (13). However, if we use a global  $\sigma$  that ensures no holes in sparse image regions, regions with high mask density tend to have overly smooth reconstructions. Therefore, in the case of subdivision mask codecs, we adapt  $\sigma$  to the local density of the mask. Unfortunately, storing individual variance values for each mask point explicitly would be too costly. Instead, we derive the local variance from the mask itself following [88]:

$$\sigma_k = (\log(1 + A_k))^p. \quad (34)$$

Here,  $\sigma_k$  is the variance at mask point  $k$  and  $p$  is a constant. To obtain  $A_k$ , we first perform a Voronoi decomposition [89] of the image with the mask points as cell centres. Then we compute  $A_k$  as the area of the Voronoi cell, which is the collection of points around a mask point  $k$  that are closer to it than any other mask point. Therefore, instead of optimising and storing individual values for  $\sigma$ , we optimise and store  $p$  instead.

We also have to optimise for the contrast parameter  $\lambda$  for the diffusivity function. As  $\lambda$  only determines the degree of anisotropy for all kernels, it does not need to be adapted locally.

Unlike RJIP, where we had a target ratio as a model parameter, we optimise our subdivision and quantisation w.r.t. a target splitting error. We first find the quantisation parameter  $q$ . To that end, we consider the curve that maps quantisation levels to the corresponding quantisation error for the original image. As the number of quantisation levels increases, the quantised image gets closer to the original image and the quantisation error decreases, which implies that the quantisation levels vs. error curve is decreasing. We select the value of  $q$  such that the curve has a derivative value of 1. This value of  $q$  is the point of diminishing return, after which increasing  $q$  does not result in a significant reduction in quantisation error. This ensures that  $q$  is large enough to have a reasonable quantisation error but not so large to have a large coding cost.

After fixing  $q$ , we perform the actual subdivision. We start at the root of the tree and reconstruct the image with just the four corner points of the image with anisotropic Shepard inpainting with optimised  $p$  and  $\lambda$  and then tonal optimisation. The parameter optimisation and tonal optimisation are alternated to adapt the parameters and the tonal values to each other so that the inpainting quality is increased. If the reconstruction error is higher than

---

**Algorithm 1** Summary of the subdivision codec with anisotropic Shepard inpainting

---

- 1: compute  $q$  from the quantisation error curve
  - 2: **while** number of nodes split  $> 0$  **do**
  - 3:     place mask points at leaf nodes
  - 4:     **while**  $n < \text{iter\_max}$ ,  $\text{iter\_max} \in \mathbb{N}$  **do**
  - 5:         optimise for  $\lambda$  and  $p$
  - 6:         perform tonal optimisation
  - 7:     compute reconstruction error at each leaf node
  - 8:     split leaf nodes with error  $>$  target splitting error
  - 9: compress tree and mask values with LPAQ
- 

the target splitting error, we split the node and go to the next level. This process of adjusting the parameters  $p$  and  $\lambda$ , the tonal optimisation, and node splitting is repeated for each tree level by going deeper into the tree until all sub-images or leaf nodes of the tree have a reconstruction error lesser than the target splitting error. Finally, the subdivision tree and the mask values are compressed by applying LPAQ2 [90]. An overview of the algorithm can be seen in Algorithm 1.

## 5. Experiments

In this section, we perform a systematic evaluation of our inpainting operators and compression pipelines in four parts. First, we compare our proposed operator to existing inpainting operators on a synthetic disc image both w.r.t. inpainting quality and runtime. Afterwards, we evaluate the scaling behaviour of the computational cost w.r.t. the number of pixels on an image from *Sintel* [91]. The third part is dedicated to a comparison of our uniform mask-based codecs to transform-based codecs on the test image *trui* and the greyscale version of the Berkeley dataset [92]. Finally, we evaluate our subdivision-based codecs on the greyscale version of the Kodak dataset [93] in comparison to JPEG.

### 5.1. Comparing Inpainting Operators

In Fig. 3, we consider the inpainting quality and computational effort on a synthetic binary disk image with a uniform mask of density 11.11%. In addition to our isotropic Shepard and anisotropic Shepard inpainting, we also consider homogeneous diffusion inpainting [26] as a baseline since it is widely used in compression applications due to its relative simplicity compared to more sophisticated diffusion inpainting. Thus, it is the direct competitor for our Shepard inpainting. To ensure a fair comparison w.r.t. timing, we use several contemporary solvers for homogeneous diffusion [19, 84].

From Fig. 3, we can see that the isotropic Shepard inpainting result yields slightly blurrier edges than homogeneous diffusion. However, the inpainting is

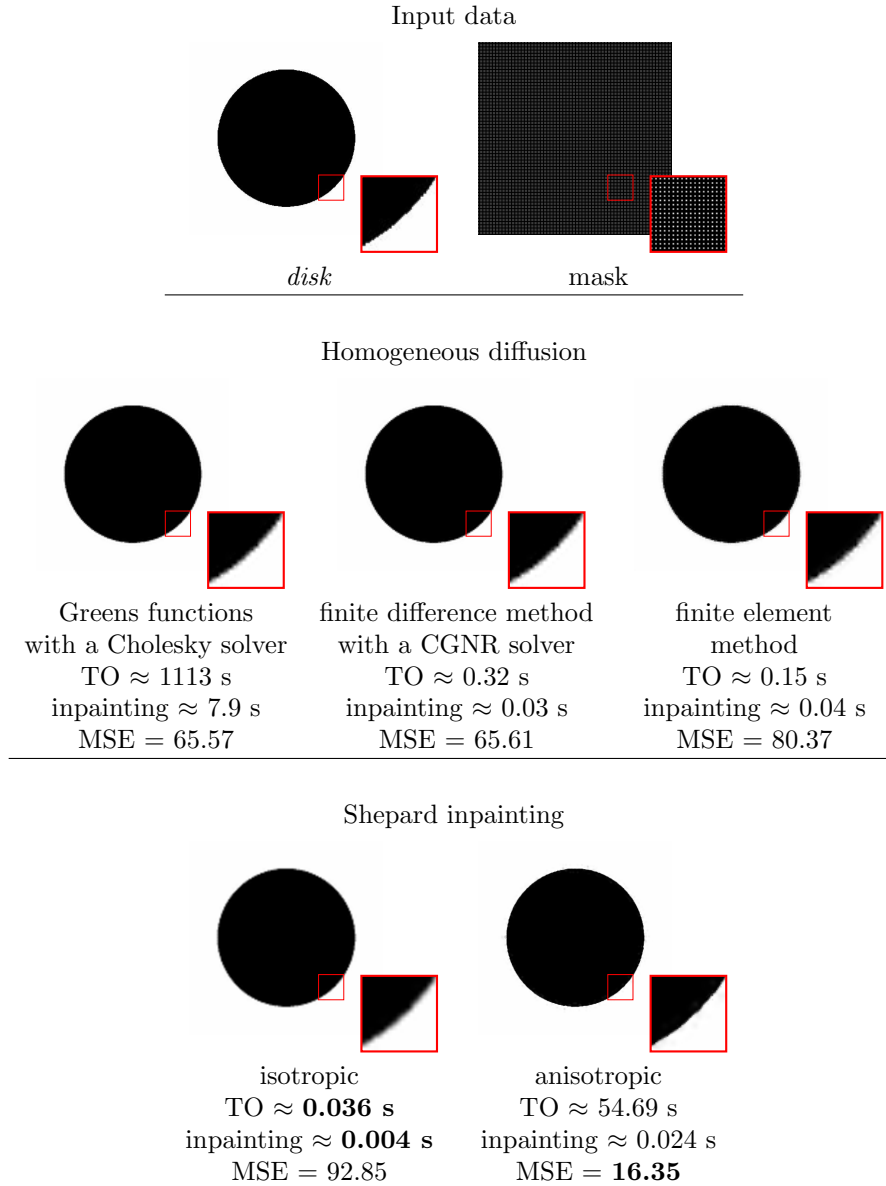


Figure 3: We compare the inpainting quality, time for tonal optimisation (TO), and inpainting time of Shepard inpainting to several contemporary solvers for homogeneous diffusion inpainting on a synthetic image of a disk of size  $400 \times 400$ . All approaches use the same uniform mask of density 11.11% (1 in 9 pixels). The experiments were run on a single core of a single core of an Intel Core i7-6700A@3.40GHz with 32 GB RAM. The experiment highlights sharper results of anisotropic Shepard inpainting compared to all competitors at an inpainting speed comparable to homogeneous diffusion. Localised isotropic Shepard inpainting can be up to an order of magnitude faster than non-localised homogeneous diffusion inpainting at a similar quality.

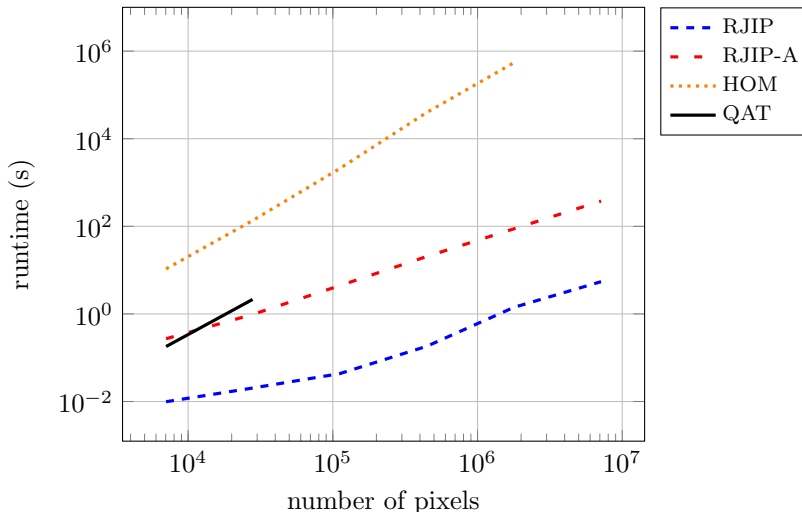


Figure 4: We compare the runtime scaling behaviour of our pipelines with homogeneous diffusion on five downsampled versions of frame 917 of the 4K CinemaScope movie *Sintel* ( $4096 \times 1744$ ). Here, both axes are presented in a log scale. The experiments are conducted on a single core of an Intel Core i7-6700A@3.40GHz with 32 GB RAM.

faster by one to three orders of magnitude. Tonal optimisation can even be faster by up to five orders of magnitude compared to the approach of Hoffmann [84]. Even the recent highly efficient finite elements method is still slower by one order of magnitude. This is a direct effect of the closed-form solution from Section 2.3 for isotropic Shepard inpainting. Thus, it constitutes a good alternative to homogeneous diffusion inpainting for time-critical applications while being significantly easier to implement.

The anisotropic version of Shepard inpainting yields much sharper results than its competitors. However, this comes at the price of a higher computational load. For pure inpainting, anisotropic Shepard is still faster than homogeneous diffusion by one to three orders of magnitude depending on the solver. However, homogeneous diffusion can be faster for tonal optimisation. Here, the anisotropy prevents the efficient closed-form solution and requires a fall-back to a simple trial-and-error algorithm. Thus, anisotropic Shepard is a good choice for pure inpainting applications and compression which requires high quality.

## 5.2. Timing Experiments

In this experiment, we investigate the scaling behaviour of our Shepard inpainting-based compression methods and homogeneous diffusion with the number of pixels. We consider RJIP and a uniform mask codec with anisotropic Shepard inpainting.

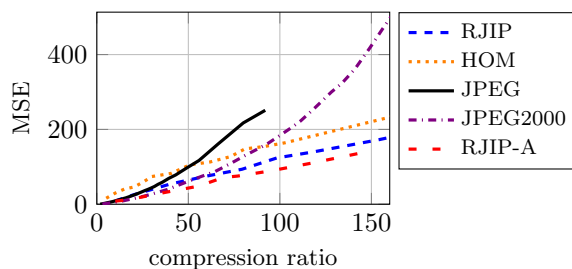
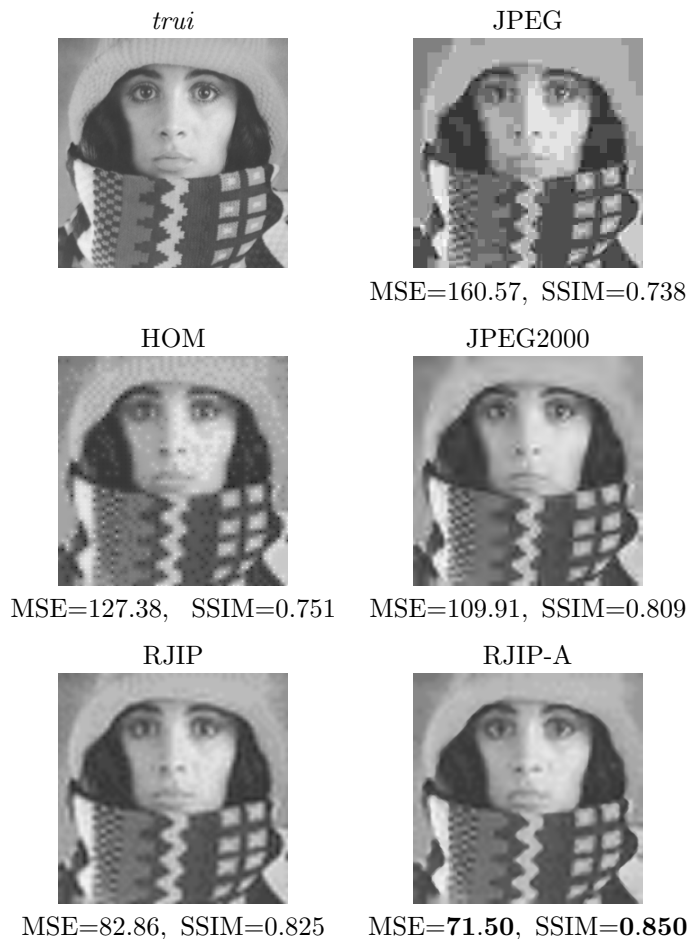
Our experiments consider a single compression with a fixed sampling distance  $r = 4$  ( $\approx 4\%$  mask density) and  $q = 32$  quantisation levels. We implemented

a version of our RJIP codec which uses homogeneous diffusion that is solved through a conjugate gradient scheme. We refer to this homogeneous diffusion version of the codec HOM. It is to be noted that our proposed tonal optimisation is not applicable to HOM, which therefore uses the simple iterative adjustment scheme. Note that also the more sophisticated tonal optimisation options for homogeneous diffusion from the previous section are not directly applicable, since they do not take quantisation into account and thus would modify the reconstruction quality. From Fig. 4, we can see that RJIP is faster than HOM by up to five orders of magnitude. The compression times for RJIP range from 0.009s for a  $128 \times 55$  image to 5.45s for a 4K image.

In contrast to RJIP, it is unpopular to localise HOM by choosing a finite stopping time, since one is usually not willing to accept the quality deterioration. Thus, the tonal optimisation is more time-consuming for non-localised homogeneous diffusion than for the localised RJIP. Peter et al. [28] proposed an alternative *quantisation-aware tonal optimisation* (QAT) which increases the speed at the cost of high memory consumption. We could not test QAT for images larger than  $512 \times 218$ , as our test machine ran out of memory. RJIP is still 2 to 3 orders of magnitude faster than this specialised algorithm.

We also implemented a uniform mask codec like RJIP, but improved it with anisotropic Shepard inpainting, which we call RJIP-A. In addition to the parameter optimisation for the grid size and the quantisation parameter, we also run an optimisation to find the contrast parameter  $\lambda$  and the variance of the Gaussians  $\sigma$  similar to our anisotropic Shepard codec on trees. For tonal optimisation, we fall back to the iterative random walk method, as a clean optimal solution for the tonal value cannot be computed here as in the case of RJIP. We also alternate the tonal and parameter optimisation to further increase quality as in Section 4.2. Finally, as we need all neighbouring pixels to compute derivatives and consequently the inpainting at that pixel, we cannot perform joint inpainting and prediction as used in RJIP. Therefore, we simply compress the pixel values with LPAQ.

We can also observe that RJIP-A is about two orders of magnitude slower than RJIP. This results from the higher amount of parameters that need to be optimised. In addition to the grid parameter  $r$  and the quantisation parameter  $q$ , we also need to determine the two additional parameters  $\lambda$  and  $\sigma$  of the anisotropic Shepard inpainting. Moreover, each individual inpainting is slower due to the computations required to calculate the Gaussian kernel at each point. Changing a pixel also requires an update of the neighbourhood derivative information. Thus, tonal optimisation is slower than for RJIP. In spite of all the additional computations, we are still faster than HOM by about one to two orders of magnitude. Furthermore, we can see that our anisotropic codec is slightly slower than QAT for very low resolutions, but quickly becomes more efficient as resolution increases.



Comparisons on the *trui* image

Figure 5: We compressed *trui* with different compression methods at a ratio of 70:1 and compare them with the MSE error measure. Additionally, we display the SSIM [94] scores for the presented images. We can see that our Shepard inpainting-based methods do not present any unpleasant artefacts. From the rate-distortion curves, we can observe that our anisotropic Shepard codec with uniform masks outperforms JPEG2000 over most compression ratios while the base RJIP codec outperforms JPEG2000 at a compression ratio of 60.

### 5.3. Comparing Uniform Mask Codecs

In this set of comparisons, we compare the base RJIP codec with isotropic Shepard inpainting on uniform masks to RJIP-A, the uniform mask codec with anisotropic Shepard inpainting. This allows us to evaluate the relative performance of the anisotropic Shepard operator on the piecewise smooth test image *trui* image and the 500 textured images of the Berkeley dataset [92]. Moreover, we also compare against JPEG and JPEG2000.

From Fig. 5, we observe that on the piecewise smooth *trui* image, RJIP-A performs the best across almost all compression ratios, even compared to JPEG2000. It benefits from its superior reconstruction of directional structures with anisotropic Shepard inpainting.

For the Berkeley dataset, this advantage is also visible for low to medium compression ratios in Fig. 6: RJIP-A outperforms its isotropic counterpart RJIP and is competitive with JPEG. At higher compression ratios, both Shepard codecs yield very similar quality and are able to beat both JPEG and JPEG2000. These very sparse mask grids contain less reliable information on anisotropy, which can cause the anisotropic Gaussian kernels to degenerate to an isotropic setting.

The more favourable rate-distortion behaviour at higher compression ratios compared to transform-based compression results from the fact that the number of mask points to be stored does not need to be reduced proportionally to the compression ratio. At high ratios, coarse quantisation can be used to reduce the coding cost, and the smooth inpainting is able to restore a wider range of grey values than that of the mask pixels. This makes our codecs particularly suited for compressing images at high compression ratios.

### 5.4. Comparing Subdivision-Based Codecs

In our final comparison, we consider the rate-distortion behaviour of our subdivision codecs for isotropic and anisotropic Shepard inpainting on the greyscale Kodak dataset. We also include the uniform mask codecs from the previous set of experiments and consider JPEG as a reference.

Our uniform mask codecs use multiple target compression ratios while we specify different target splitting errors for our subdivision codecs to steer the rate-distortion trade-off. For this set of experiments, we present images that show representative performance for different image content and different behaviour of our algorithms in Fig. 6. The rate-distortion curves for all images in the Kodak dataset can be found in the supplementary material.

Fig. 6 illustrates that for images with a dominant foreground and a homogeneous background, the subdivision codecs outperform their regular grid counterparts. In such images, the subdivision codecs benefit from denser known data in textured regions. This also leads to a higher accuracy of the derivative approximations for anisotropic Shepard inpainting in such dense regions,

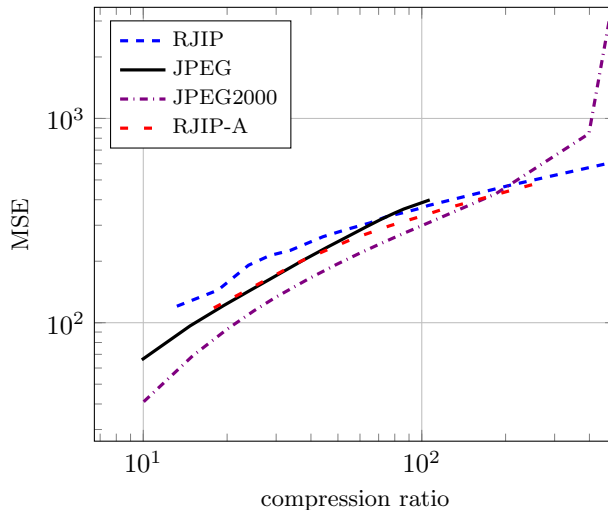


Figure 6: On the Berkeley database with textured images, RJIP-A is competitive to JPEG at low compression ratios whereas RJIP and RJIP-A outperforms JPEG and JPEG2000 for high compression ratios. Both axes in the plot are presented in a log scale.

yielding a better overall reconstruction quality. Even at higher compression ratios, our subdivision codecs can retain more structures compared to the original RJIP codec.

On the other hand, for images that are highly textured overall, the advantages of the subdivision codec diminish. Since all regions are similarly detailed, it produces uniformly distributed masks and thus degenerates to the uniform codec. However, it still requires significant overhead for the tree structure and thus performs worse than its simpler counterpart. This suggests switching between both coding archetypes depending on the image content.

## 6. Conclusions and Outlook

We have presented a family of simple but efficient image compression methods that are based on Shepard inpainting. It illustrates that straightforward inpainting methods can become competitive if they are equipped with carefully chosen components. Joint inpainting and prediction is a novel concept that increases coding efficiency at no additional storage overhead. While it thrives in combination with very efficient inpainting approaches such as Shepard interpolation, it can also be integrated in other future inpainting-based approaches.

Furthermore, our anisotropic Shepard extension demonstrates that sharp reconstructions from sparse data are possible at fast runtimes that are so far only associated with sophisticated implementations of linear diffusion inpainting. Due to its ease of implementation, anisotropic Shepard inpainting offers an alternative for future practical applications. In particular, for images with



*kodim23*



JPEG

ratio 116:1, MSE = 124.63



uniform isotropic (RJIP)  
ratio 117:1, MSE = 113.06



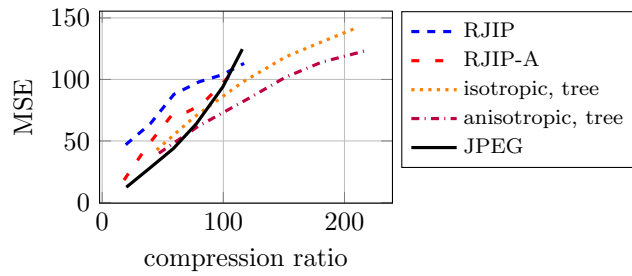
tree isotropic  
ratio 116:1, MSE = 97.82



uniform anisotropic (RJIP-A)  
ratio 109:1, MSE = 107.10



tree anisotropic  
ratio 120:1, MSE = **83.93**



rate-distortion comparisons for *kodim23*

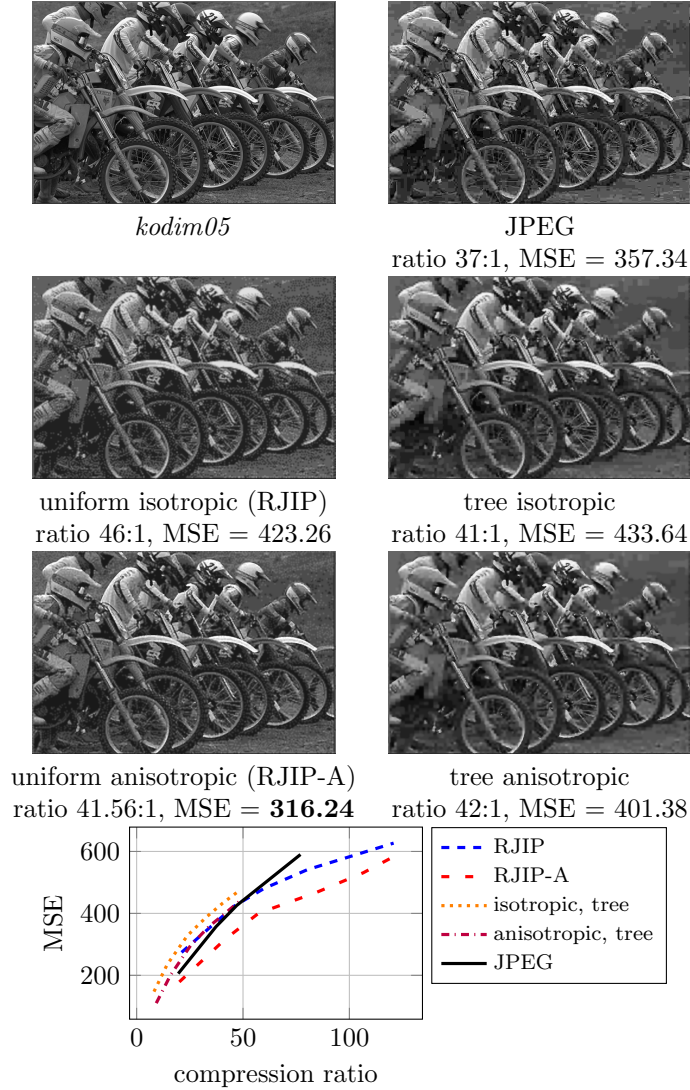


Figure 6: Our anisotropic Shepard inpainting-based codecs perform better than their isotropic counterparts overall and outperform JPEG at higher compression ratios. From the plots, we can see that the subdivision-based codecs perform better than the regular mask-based codecs if the image has a clear foreground subject. This is caused by the fact that they can adapt the mask such that the detailed regions are reconstructed better. On the other hand, the regular mask-based codecs perform better if the image is textured overall.

clearly separated fore- and background, it performs well in combination with our adaptive subdivision schemes.

In general, the straightforward Shepard codecs are competitive with existing transform-based codecs for high compression ratios. They do not produce block artefacts even with very little stored data and can also outperform both JPEG and JPEG2000 quantitatively, especially on piecewise-smooth images.

In the future, we aim to extend our Shepard-based codecs to colour images by employing dedicated strategies that exploit human perception. As Shepard inpainting excels on piecewise smooth data, we hope that it contributes to the compression of depth maps or flow fields. First attempts that followed our earlier conference publication [25] already yielded promising results [10].

#### *Acknowledgements*

We thank Vassillen Chizhov for providing his implementation of Voronoi decomposition, which was integrated into the subdivision-based anisotropic Shepard codec. We also thank Dr Matthias Augustin for his implementation of the Green's functions implementation of tonal optimisation for homogeneous diffusion [84], which was used for comparisons in Section 5.1.

#### **References**

- [1] S. Masnou, J.-M. Morel, Level lines based disocclusion, in: Proc. 1998 IEEE International Conference on Image Processing, Vol. 3, Chicago, IL, 1998, pp. 259–263. doi:10.1109/ICIP.1998.999016.
- [2] A. A. Efros, T. K. Leung, Texture synthesis by non-parametric sampling, in: Proc. Seventh IEEE International Conference on Computer Vision, Vol. 2, Corfu, Greece, 1999, pp. 1033–1038. doi:10.1109/ICCV.1999.790383.
- [3] M. Bertalmío, G. Sapiro, V. Caselles, C. Ballester, Image inpainting, in: Proc. SIGGRAPH 2000, New Orleans, LI, 2000, pp. 417–424. doi:10.1145/344779.344972.
- [4] I. Galić, J. Weickert, M. Welk, A. Bruhn, A. Belyaev, H.-P. Seidel, Image compression with anisotropic diffusion, *Journal of Mathematical Imaging and Vision* 31 (2–3) (2008) 255–269. doi:10.1007/s10851-008-0087-0.
- [5] C. Schmaltz, P. Peter, M. Mainberger, F. Ebel, J. Weickert, A. Bruhn, Understanding, optimising, and extending data compression with anisotropic diffusion, *International Journal of Computer Vision* 108 (3) (2014) 222–240. doi:10.1007/s11263-014-0702-z.
- [6] H. Werner, Studies on contour, *The American Journal of Psychology* 47 (1) (1935) 40–64. doi:10.2307/1416707.
- [7] W. B. Pennebaker, J. L. Mitchell, *JPEG: Still Image Data Compression Standard*, Springer, New York, 1992.

- [8] C. Christopoulos, A. Skodras, T. Ebrahimi, The JPEG2000 still image coding system: an overview, *IEEE Transactions on Consumer Electronics* 46 (4) (2000) 1103–1127. doi:10.1109/30.920468.
- [9] F. Bellard, BPG specification, [http://bellard.org/bpg/bpg\\_spec.txt](http://bellard.org/bpg/bpg_spec.txt), last checked: 2024-06-07 (2014).
- [10] F. Jost, P. Peter, J. Weickert, Compressing piecewise smooth images with the Mumford–Shah cartoon model, in: *Proc. 28th European Signal Processing Conference*, Amsterdam, Netherlands, 2021, pp. 511–515. doi:10.23919/Eusipco47968.2020.9287790.
- [11] L. Karos, P. Bheed, P. Peter, J. Weickert, Optimising data for exemplar-based inpainting, in: J. Blanc-Talon, D. Helbert, W. Philips, D. Popescu, P. Scheunders (Eds.), *Advanced Concepts for Intelligent Vision Systems*, Vol. 11182 of *Lecture Notes in Computer Science*, Springer, Cham, 2018, pp. 547–558. doi:10.1007/978-3-030-01449-0\_46.
- [12] V. Daropoulos, M. Augustin, J. Weickert, Sparse inpainting with smoothed particle hydrodynamics, *SIAM Journal on Imaging Sciences* 14 (4) (2021) 1669–1705. doi:10.1137/20M1382179.
- [13] R. Distasi, M. Nappi, S. Vitulano, Image compression by B-tree triangular coding, *IEEE Transactions on Communications* 45 (9) (1997) 1095–1100. doi:10.1109/26.623074.
- [14] L. Demaret, N. Dyn, A. Iske, Image compression by linear splines over adaptive triangulations, *Signal Processing* 86 (7) (2006) 1604–1616. doi:10.1016/j.sigpro.2005.09.003.
- [15] D. Marwood, P. Massimino, M. Covell, S. Baluja, Representing images in 200 bytes: Compression via triangulation, in: *Proc. 25th IEEE International Conference on Image Processing*, Athens, Greece, 2018, pp. 405–409. doi:10.1109/ICIP.2018.8451393.
- [16] H. Köstler, M. Stürmer, C. Freundl, U. Råde, PDE based video compression in real time, *Tech. Rep. 07-11*, Lehrstuhl für Informatik 10, University Erlangen–Nürnberg, Germany (2007).
- [17] M. Mainberger, A. Bruhn, J. Weickert, S. Forchhammer, Edge-based compression of cartoon-like images with homogeneous diffusion, *Pattern Recognition* 44 (9) (2011) 1859–1873. doi:10.1016/j.patcog.2010.08.004.
- [18] S. Hoffmann, G. Plonka, J. Weickert, Discrete Green’s functions for harmonic and biharmonic inpainting with sparse atoms, in: X.-C. Tai, E. Bae, T. F. Chan, M. Lysaker (Eds.), *Energy Minimization Methods in Computer Vision and Pattern Recognition*, Vol. 8932 of *Lecture Notes in Computer Science*, Springer, Berlin, 2015, pp. 169–182. doi:10.1007/978-3-319-14612-6\_13.

- [19] V. Chizhov, J. Weickert, Efficient data optimisation for harmonic inpainting with finite elements, in: N. Tsapatsoulis, A. Panayides, T. Theodoridis, A. Lanitis, C. Pattichis, M. Vento (Eds.), *Computer Analysis of Images and Patterns*, Springer, Cham, 2021, pp. 432–441. doi:10.1007/978-3-030-89131-2\_40.
- [20] E. M. Kalmoun, M. M. S. Nasser, Harmonic image inpainting using the charge simulation method, *Pattern Analysis and Applications* 25 (4) (2022) 795–806. doi:10.1007/s10044-022-01074-3.
- [21] N. Kämper, J. Weickert, Domain decomposition algorithms for real-time homogeneous diffusion inpainting in 4K, in: *Proc. 2022 IEEE International Conference on Acoustics, Speech and Signal Processing*, 2022, pp. 1680–1684. doi:10.1109/ICASSP43922.2022.9746831.
- [22] D. Shepard, A two-dimensional interpolation function for irregularly-spaced data, in: *Proc. 23rd ACM National Conference*, Las Vegas, NV, 1968, pp. 517–524. doi:10.1145/800186.810616.
- [23] P. Peter, C. Schmaltz, N. Mach, M. Mainberger, J. Weickert, Beyond pure quality: Progressive modes, region of interest coding, and real time video decoding for PDE-based image compression., *Journal of Visual Communication and Image Representation* 31 (4) (2015) 253–265. doi:10.1016/j.jvcir.2015.06.017.
- [24] R. Achanta, N. Arvanitopoulos, S. Süsstrunk, Extreme image completion, in: *Proc. 42nd IEEE International Conference on Acoustics, Speech and Signal Processing*, New Orleans, LA, 2017, pp. 1333–1337. doi:10.1109/icassp.2017.7952373.
- [25] P. Peter, Fast inpainting-based compression: Combining Shepard interpolation with joint inpainting and prediction, in: *Proc. 26th IEEE International Conference on Image Processing*, Taipei, Taiwan, 2019, pp. 3557–3561. doi:10.1109/icip.2019.8803760.
- [26] T. Iijima, Basic theory on normalization of pattern (in case of typical one-dimensional pattern), *Bulletin of the Electrotechnical Laboratory* 26 (1962) 368–388, in Japanese.
- [27] S. Hoffmann, M. Mainberger, J. Weickert, M. Puhl, Compression of depth maps with segment-based homogeneous diffusion, in: A. Kuijper, K. Bredies, T. Pock, H. Bischof (Eds.), *Scale-Space and Variational Methods in Computer Vision*, Vol. 7893 of *Lecture Notes in Computer Science*, Springer, Berlin, 2013, pp. 319–330. doi:10.1007/978-3-642-38267-3\_27.
- [28] P. Peter, S. Hoffmann, F. Nedwed, L. Hoeltgen, J. Weickert, Evaluating the true potential of diffusion-based inpainting in a compression context, *Signal Processing: Image Communication* 46 (2016) 40–53. doi:10.1016/j.image.2016.05.002.

- [29] S. Carlsson, Sketch based coding of grey level images, *Signal Processing* 15 (1) (1988) 57–83. doi:10.1016/0165-1684(88)90028-X.
- [30] J. Gautier, O. Le Meur, C. Guillemot, Efficient depth map compression based on lossless edge coding and diffusion, in: *Proc. 29th Picture Coding Symposium*, Kraków, Poland, 2012, pp. 81–84. doi:10.1109/PCS.2012.6213291.
- [31] F. Jost, P. Peter, J. Weickert, Compressing flow fields with edge-aware homogeneous diffusion inpainting, in: *Proc. 45th International Conference on Acoustics, Speech, and Signal Processing*, Barcelona, Spain, 2020, pp. 2198–2202. doi:10.1109/ICASSP40776.2020.9054255.
- [32] J. Duchon, Interpolation des fonctions de deux variables suivant le principe de la flexion des plaques minces, *Revue française d’automatique, informatique, recherche opérationnelle. Analyse numérique* 10 (3) (1976) 5–12. doi:10.1051/m2an/197610R300051.
- [33] Y. Chen, R. Ranftl, T. Pock, A bi-level view of inpainting-based image compression, in: Z. Kúkelová, J. Heller (Eds.), *Proc. 19th Computer Vision Winter Workshop*, Křtiny, Czech Republic, 2014, pp. 19–26.
- [34] J. Weickert, Theoretical foundations of anisotropic diffusion in image processing, *Computing Supplement* 11 (1996) 221–236. doi:10.1007/978-3-7091-6586-7\_13.
- [35] J. Weickert, M. Welk, Tensor field interpolation with PDEs, in: J. Weickert, H. Hagen (Eds.), *Visualization and Processing of Tensor Fields*, Springer, Berlin, 2006, pp. 315–325. doi:10.1007/3-540-31272-2\_19.
- [36] P. Peter, L. Kaufhold, J. Weickert, Turning diffusion-based image colorization into efficient color compression, *IEEE Transactions on Image Processing* 26 (2) (2016) 860–869. doi:10.1109/TIP.2016.2627800.
- [37] I. Jumakulyyev, T. Schulz, Fourth-order anisotropic diffusion for inpainting and image compression, in: E. Özarslan, T. Schulz, E. Zhang, A. Fuster (Eds.), *Anisotropy Across Fields and Scales*, Springer, Cham, 2021, pp. 99–124. doi:10.1007/978-3-030-56215-1\_5.
- [38] G. Facciolo, P. Arias, V. Caselles, G. Sapiro, Exemplar-based interpolation of sparsely sampled images, in: D. Cremers, Y. Boykov, A. Blake, F. R. Schmidt (Eds.), *Energy Minimisation Methods in Computer Vision and Pattern Recognition*, Vol. 5681 of *Lecture Notes in Computer Science*, Springer, Berlin, 2009, pp. 331–344. doi:10.1007/978-3-642-03641-5\_25.
- [39] P. Peter, J. Weickert, Compressing images with diffusion- and exemplar-based inpainting, in: J.-F. Aujol, M. Nikolova, N. Papadakis (Eds.), *Scale-Space and Variational Methods in Computer Vision*, Vol. 9087 of *Lecture*

- Notes in Computer Science, Springer, Berlin, 2015, pp. 154–165. doi: 10.1007/978-3-319-18461-6\_13.
- [40] J. Xie, L. Xu, E. Chen, Image denoising and inpainting with deep neural networks, in: P. L. Bartlett, F. C. N. Pereira, C. J. C. Burges, L. Bottou, K. Q. Weinberger (Eds.), Proc. 26th International Conference on Neural Information Processing Systems, Vol. 25 of Advances in Neural Information Processing Systems, Lake Tahoe, NV, 2012, pp. 350–358.
- [41] D. Pathak, P. Krähenbühl, J. Donahue, T. Darrell, A. A. Efros, Context encoders: Feature learning by inpainting, in: Proc. 2016 IEEE Conference on Computer Vision and Pattern Recognition, Las Vegas, NV, 2016, pp. 2536–2544. doi:10.1109/CVPR.2016.278.
- [42] C. Yang, X. Lu, Z. Lin, E. Shechtman, O. Wang, H. Li, High-resolution image inpainting using multi-scale neural patch synthesis, in: Proc. 2017 IEEE Conference on Computer Vision and Pattern Recognition, Honolulu, HI, 2017, pp. 6721–6729. doi:10.1109/CVPR.2017.434.
- [43] D. Vařata, T. Halama, M. Friedjungová, Image inpainting using Wasserstein generative adversarial imputation network, in: I. Farkaš, P. Masulli, S. Otte, S. Wermter (Eds.), Artificial Neural Networks and Machine Learning – ICANN 2021, Vol. 12892 of Lecture Notes in Computer Science, Springer, Cham, 2021, pp. 575–586. doi:10.1007/978-3-030-86340-1\_46.
- [44] P. Peter, A Wasserstein GAN for joint learning of inpainting and its spatial optimisation, in: H. Wang, W. Lin, P. Manoranjan, G. Xiao, K. P. Chan, X. Wang, G. Ping, H. Jiang (Eds.), Image and Video Technology, Vol. 13763 of Lecture Notes in Computer Science, Springer International Publishing, Cham, 2023, pp. 132–145. doi:10.1007/978-3-031-26431-3\_11.
- [45] V. Lempitsky, A. Vedaldi, D. Ulyanov, Deep image prior, in: 2018 IEEE/CVF Conference on Computer Vision and Pattern Recognition, Salt Lake City, UT, 2018, pp. 9446–9454. doi:10.1109/CVPR.2018.00984.
- [46] R. L. Hardy, Multiquadric equations of topography and other irregular surfaces, *Journal of Geophysical Research* 76 (8) (1971) 1905–1915. doi: 10.1029/JB076i008p01905.
- [47] M. D. Buhmann, Radial Basis Functions: Theory and Implementations, Vol. 12, Cambridge University Press, Cambridge, UK, 2003. doi:10.1017/CB09780511543241.
- [48] F. Magoulès, L. A. Diago, I. Hagiwara, A two-level iterative method for image reconstruction with radial basis functions, *JSME International Journal Series C, Mechanical Systems, Machine Elements and Manufacturing* 48 (2) (2005) 149–158. doi:10.1299/jsmec.48.149.

- [49] H. Wendland, *Scattered Data Approximation*, Cambridge University Press, Cambridge, UK, 2005. doi:10.1017/CB09780511617539.
- [50] M. Augustin, J. Weickert, S. Andris, Pseudodifferential inpainting: The missing link between PDE- and RBF-based interpolation, in: J. Lellmann, M. Burger, J. Modersitzki (Eds.), *Scale Space and Variational Methods in Computer Vision*, Springer, Cham, 2019, pp. 67–78. doi:10.1007/978-3-030-22368-7\_6.
- [51] G. Di Blasi, E. Francomano, A. Tortorici, E. Toscano, A smoothed particle image reconstruction method, *Calcolo* 48 (1) (2011) 61–74. doi:10.1007/s10092-010-0028-3.
- [52] R. Beatson, O. Davydov, J. Levesley, Error bounds for anisotropic RBF interpolation, *Journal of Approximation Theory* 162 (3) (2010) 512–527. doi:10.1016/j.jat.2009.08.004.
- [53] G. Casciola, L. B. Montefusco, S. Morigi, Edge-driven image interpolation using adaptive anisotropic radial basis functions, *Journal of Mathematical Imaging and Vision* 36 (2) (2010) 125–139. doi:10.1007/s10851-009-0176-8.
- [54] R. Franke, G. Nielson, Smooth interpolation of large sets of scattered data, *Numerical Methods in Engineering* 15 (11) (1980) 1691–1704. doi:10.1002/nme.1620151110.
- [55] R. J. Renka, Multivariate interpolation of large sets of scattered data, *ACM Transactions on Mathematical Software* 14 (2) (1988) 139–148. doi:10.1145/45054.45055.
- [56] Z. Li, X. Zhang, R. Zhu, Z. Zhang, Z. Weng, Integrating data-to-data correlation into inverse distance weighting, *Computational Geosciences* 24 (2019) 203–216. doi:10.1007/s10596-019-09913-9.
- [57] M. Tomczak, Spatial interpolation and its uncertainty using automated anisotropic inverse distance weighting (IDW)–cross–validation/jackknife approach, *Journal of Geographic Information and Decision Analysis* 2 (2) (1998) 18–30.
- [58] E. Ringaby, O. Friman, P.-E. Forssén, T. O. Opsahl, T. V. Haavardsholm, I. Käsen, Anisotropic scattered data interpolation for pushbroom image rectification, *IEEE Transactions on Image Processing* 23 (5) (2014) 2302–2314. doi:10.1109/TIP.2014.2316377.
- [59] J. M. Lorenzi, T. Stecher, K. Reuter, S. Matera, Local-metrics error-based Shepard interpolation as surrogate for highly non-linear material models in high dimensions, *Journal of Chemical Physics* 147 (16), article no. 164106. doi:10.1063/1.4997286.

- [60] H. Knutsson, C.-F. Westin, Normalized and differential convolution, in: Proc. 1993 IEEE Conference on Computer Vision and Pattern Recognition, New York, NY, 1993, pp. 515–523. doi:10.1109/CVPR.1993.341081.
- [61] Z. Belhachmi, D. Bucur, B. Burgeth, J. Weickert, How to choose interpolation data in images, SIAM Journal on Applied Mathematics 70 (1) (2009) 333–352. doi:10.1137/080716396.
- [62] M. Mainberger, S. Hoffmann, J. Weickert, C. H. Tang, D. Johannsen, F. Neumann, B. Doerr, Optimising spatial and tonal data for homogeneous diffusion inpainting., in: A. Bruckstein, B. ter Haar Romeny, A. Bronstein, M. Bronstein (Eds.), Scale Space and Variational Methods in Computer Vision, Vol. 6667 of Lecture Notes in Computer Science, Springer, Berlin, 2011, pp. 26–37. doi:10.1007/978-3-642-24785-9\_3.
- [63] G. Albanese, M. Cipolla, C. Valenti, Genetic normalized convolution, in: G. Maino, G. L. Foresti (Eds.), International Conference on Image Analysis and Processing, Vol. 6978 of Lecture Notes in Computer Science, Springer, Berlin, Heidelberg, 2011, pp. 670–679. doi:10.1007/978-3-642-24085-0\_68.
- [64] L. Hoeltgen, S. Setzer, J. Weickert, An optimal control approach to find sparse data for Laplace interpolation, in: A. Heyden, F. Kahl, C. Olsson, M. Oskarsson, X.-C. Tai (Eds.), Energy Minimization Methods in Computer Vision and Pattern Recognition, Vol. 8081 of Lecture Notes in Computer Science, Springer, Berlin, 2013, pp. 151–164. doi:10.1007/978-3-642-40395-8\_12.
- [65] S. Bonettini, I. Loris, F. Porta, M. Prato, S. Rebegoldi, On the convergence of a linesearch based proximal-gradient method for nonconvex optimization, Inverse Problems 33 (055005). doi:10.1088/1361-6420/aa5bfd.
- [66] Q. Dai, H. Chopp, E. Pouyet, O. Cossairt, M. Walton, A. K. Katsaggelos, Adaptive image sampling using deep learning and its application on X-Ray fluorescence image reconstruction, IEEE Transactions on Multimedia 22 (10) (2019) 2564–2578. doi:10.1109/TMM.2019.2958760.
- [67] M. Breuß, L. Hoeltgen, G. Radow, Towards PDE-based video compression with optimal masks prolonged by optic flow, Journal of Mathematical Imaging and Vision 63 (2) (2020) 144–156. doi:10.1007/s10851-020-00973-6.
- [68] P. Peter, K. Schrader, T. Alt, J. Weickert, Deep spatial and tonal data optimisation for homogeneous diffusion inpainting, Pattern Analysis and Applications 26 (4) (2023) 1585–1600. doi:10.1007/s10044-023-01162-y.
- [69] R. M. K. Mohideen, P. Peter, J. Weickert, A systematic evaluation of coding strategies for sparse binary images, Signal Processing: Image Communication 99 (2021) 116424. doi:10.1016/j.image.2021.116424.

- [70] L. Hoeltgen, M. Mainberger, S. Hoffmann, J. Weickert, C. H. Tang, S. Setzer, D. Johannsen, F. Neumann, B. Doerr, Optimising spatial and tonal data for PDE-based inpainting, in: M. Bergounioux, G. Peyré, C. Schnörr (Eds.), *Variational Methods in Image Analysis*, De Gruyter, Berlin, 2016, pp. 35–83. doi:10.1515/9783110430394-002.
- [71] M. Mahoney, Adaptive weighing of context models for lossless data compression, Tech. Rep. CS-2005-16, Florida Institute of Technology, Melbourne, FL (Dec. 2005).
- [72] J. G. Cleary, I. H. Witten, Data compression using adaptive coding and partial string matching, *IEEE Transactions on Communications* 32 (4) (1984) 396–402. doi:10.1109/TCOM.1984.1096090.
- [73] L. D. Crocker, PNG: The portable network graphic format, *Dr. Dobb's Journal – Software Tools for the Professional Programmer* 20 (7) (1995) 36–45.
- [74] P. Perona, J. Malik, Scale space and edge detection using anisotropic diffusion, *IEEE Transactions on Pattern Analysis and Machine Intelligence* 12 (7) (1990) 629–639. doi:10.1109/34.56205.
- [75] J. Weickert, *Anisotropic Diffusion in Image Processing*, Teubner, Stuttgart, 1998.
- [76] P. Charbonnier, L. Blanc-Féraud, G. Aubert, M. Barlaud, Two deterministic half-quadratic regularization algorithms for computed imaging, in: *Proc. First IEEE International Conference on Image Processing*, Vol. 2, Austin, TX, 1994, pp. 168–172. doi:10.1109/ICIP.1994.413553.
- [77] K. W. Morton, L. M. Meyers, *Numerical Solution of Partial Differential Equations*, 2nd Edition, Cambridge University Press, Cambridge, UK, 2005. doi:10.1017/CB09780511812248.011.
- [78] J. Weickert, S. Grewenig, C. Schroers, A. Bruhn, Cyclic schemes for PDE-based image analysis, *International Journal of Computer Vision* 118 (3) (2015) 275–299. doi:10.1007/s11263-015-0874-1.
- [79] D. Hafner, P. Ochs, J. Weickert, M. Reißel, S. Grewenig, FSI schemes: Fast semi-iterative solvers for PDEs and optimisation methods, in: B. Rosenhahn, B. Andres (Eds.), *Pattern Recognition*, Vol. 9796 of *Lecture Notes in Computer Science*, Springer International Publishing, Cham, 2016, pp. 91–102. doi:10.1007/978-3-319-45886-1\_8.
- [80] J. A. Tómasson, P. Ochs, J. Weickert, AFSI: Adaptive restart for fast semi-iterative schemes for convex optimisation, in: T. Brox, A. Bruhn, M. Fritz (Eds.), *Pattern Recognition*, Vol. 11269 of *Lecture Notes in Computer Science*, Springer International Publishing, Cham, 2019, pp. 669–681. doi:10.1007/978-3-030-12939-2\_46.

- [81] L. Bergerhoff, J. Weickert, Y. Dar, Algorithms for piecewise constant signal approximations, in: Proc. 27th European Signal Processing Conference, A Coruña, Spain, 2019. doi:10.23919/EUSIPCO.2019.8902559.
- [82] Y. Dar, A. M. Bruckstein, On high-resolution adaptive sampling of deterministic signals, Journal of Mathematical Imaging and Vision 61 (7) (2019) 944–966. doi:10.1007/s10851-019-00880-5.
- [83] R. D. Adam, P. Peter, J. Weickert, Denoising by inpainting, in: F. Lauze, Y. Dong, A. B. Dahl (Eds.), Scale Space and Variational Methods in Computer Vision, Vol. 10302 of Lecture Notes in Computer Science, Springer, Cham, 2017, pp. 121–132. doi:10.1007/978-3-319-58771-4\_10.
- [84] S. Hoffmann, Competitive image compression with linear PDEs, Ph.D. thesis, Faculty of Mathematics and Computer Science, Saarland University (2016).
- [85] Y. Collet, Finite state entropy (FSE) implementation, <https://github.com/Cyan4973/FiniteStateEntropy>, last checked: 2024-06-03 (2014).
- [86] I. H. Witten, R. M. Neal, J. G. Cleary, Arithmetic coding for data compression, Communications of the ACM 30 (6) (1987) 520–540. doi:10.1145/214762.214771.
- [87] R. M. K. Mohideen, P. Peter, T. Alt, J. Weickert, A. Scheer, Compressing colour images with joint inpainting and prediction, arXiv:2010.09866 [eess.IV] (Oct. 2020). doi:10.48550/arXiv.2010.09866.
- [88] L. Wang, B. Hua, X. Li, Adaptive energy diffusion for blind inverse halftoning, in: G. Qiu, K. M. Lam, H. Kiya, X. Xue, C. J. Kuo, M. S. Lew (Eds.), Advances in Multimedia Information Processing - PCM 2010, Vol. 6297 of Lecture Notes in Computer Science, Springer, Berlin, Heidelberg, 2010, pp. 470–480. doi:10.1007/978-3-642-15702-8\_43.
- [89] F. Aurenhammer, R. Klein, D. Lee, Voronoi Diagrams and Delaunay Triangulations, World Scientific Publishing Company, 2013. doi:10.1142/8685.
- [90] M. Mahoney, LPAQ, <http://mattmahoney.net/dc/#lpaq>, last checked: 2024-06-03 (2007).
- [91] T. Roosendaal, Sintel, in: ACM SIGGRAPH 2011 Computer Animation Festival, Association for Computing Machinery, New York, NY, USA, 2011, p. 71. doi:10.1145/2019001.2019066.
- [92] D. Martin, C. Fowlkes, D. Tal, J. Malik, A database of human segmented natural images and its application to evaluating segmentation algorithms and measuring ecological statistics, in: Proc. Eighth International Conference on Computer Vision, Vol. 2, Vancouver, Canada, 2001, pp. 416–423. doi:10.1109/ICCV.2001.937655.

- [93] E. K. Company, Kodak true color image suite, <http://r0k.us/graphics/kodak/>, last checked: 2024-06-03 (1999).
- [94] Z. Wang, A. C. Bovik, H. R. Sheikh, E. P. Simoncelli, Image quality assessment: From error visibility to structural similarity, *IEEE Transactions on Image Processing* 13 (4) (2004) 600–612. doi:10.1109/TIP.2003.819861.

## Supplementary Material

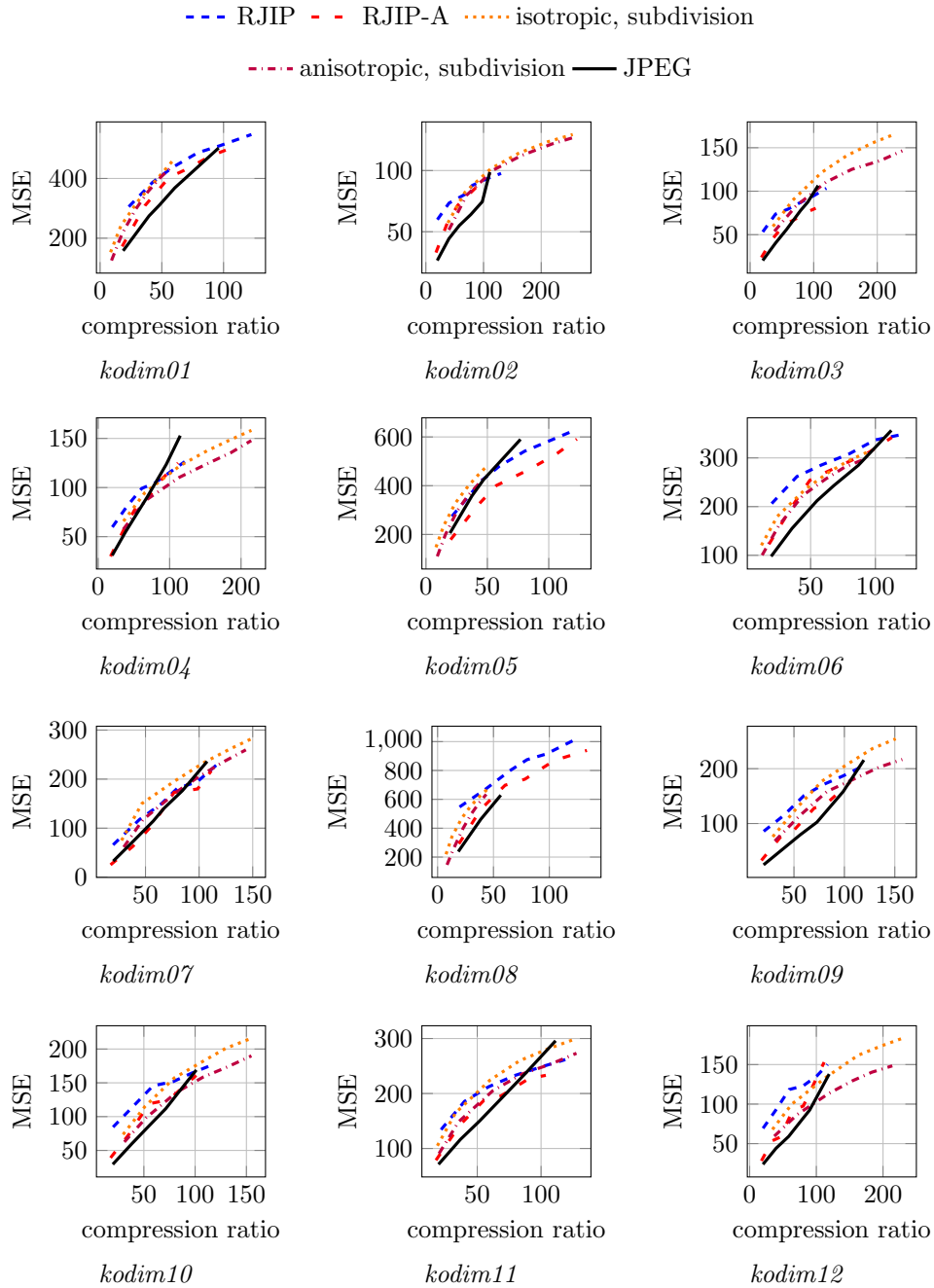


Figure 7: Rate-distortion comparisons on the Kodak database

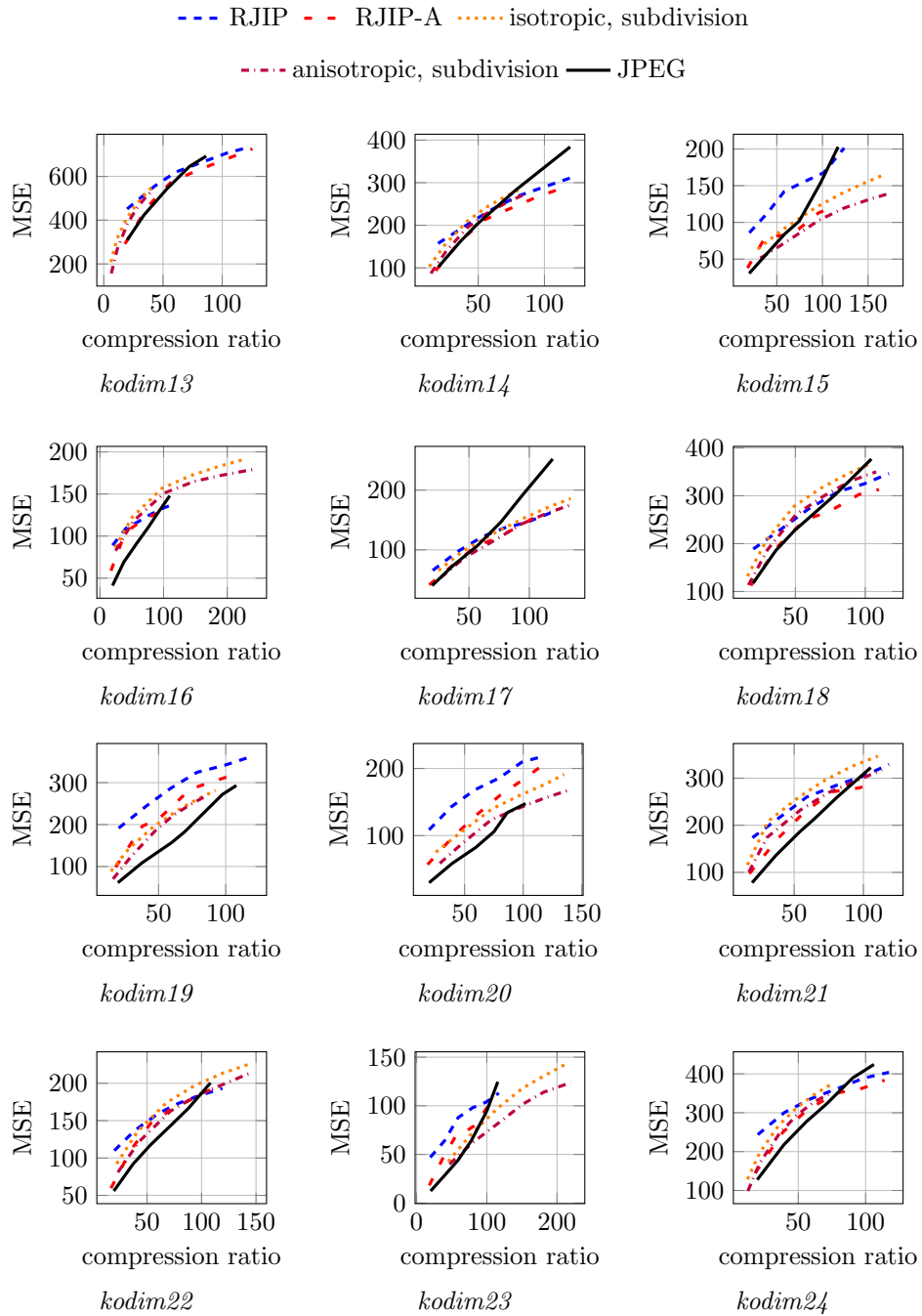


Figure 8: Rate-distortion comparisons on the Kodak database